Available online at ScienceDirect

ScienceDirect

J. Mater. Sci. Technol., 2014, 30(12), 1243−1250

JMST

www.JMST.org

Mechanical Properties and Microstructure of 6082-T6 Aluminum Alloy Joints by Self-support Friction Stir Welding

Long Wan, Yongxian Huang, Weiqiang Guo, Shixiong Lv, Jicai Feng*

State Key Laboratory of Advanced Welding and Joining, Harbin Institute of Technology, Harbin 150001, China

[Manuscript received December 17, 2013, in revised form February 23, 2014, Available online 19 April 2014]

The majority of this research has concentrated on developing the self-support friction stir welding (SSFSW) tool which consists of a big concave upper shoulder and a small convex lower shoulder, and procedures for making reliable welds in aluminum hollow extrusion. The 5-mm-thick 6082-T6 aluminum alloy was self-support friction stir welded at a constant tool rotation speed of 800 r/min. The effect of welding speed on microstructure and mechanical properties was investigated. The results of transverse tensile test indicated that the tensile strength of joints increased and the elongation decreased with increasing welding speed. The whole values of microhardness of SSFSW joints increased with increasing welding speed from 10 to 200 mm/min. The defect-free joints were obtained at lower welding speeds and the tensile fracture was located at the heat-affected zone (HAZ) adjacent to the thermo-mechanically affected zone (TMAZ) on the advancing side. The investigation of the flow pattern of the softened metal around the SSFSW tool revealed that the flow pattern of the softened metal was driven by two shoulders and the stir pin. The failure of specimens in tension presented the ductile fracture mode.

KEY WORDS: Self-support friction stir welding; Aluminum alloy; Welding speed; Mechanical properties; Microstructure; Flow pattern

1. Introduction

Friction stir welding (FSW) was developed in 1991 and has rapidly become an important process for joining aluminum alloys, as a solid-state welding process that offers an attractive alternative to fusion welding[1,2]. Because no melting occurs during FSW, the process is performed at much lower temperatures than conventional welding techniques and circumvents many of the environmental and safety issues associated with these welding methods[3]. In recent decades, the railway vehicle bodies made of aluminum hollow extrusions, integrating the functions of beams and plates because of its high rigidity, are now getting popular to reduce their weight and improve their environmental impact[4]. The application of double skinned structure shortens the length of the welding line because the extrusions are aligned longitudinally and provides greater flexibility in the choice of cross-section of the car body[5]. The FSW technique is currently applied to the construction of double skinned railway vehicles made of aluminum hollow extrusions[6]. However, root flaws due to a lack of tool penetration are possible to exist and a high force has to be generated to react against the welding tool pressure load. It is necessary to have a device of high rigidity and profiled backing bar to achieve conventional FSW successfully[6−8].

Consequently, the bobbin tool friction stir welding (BTFSW) technique (also named as self-reacting friction stir welding, SRFSW) is developed by employing a bottom shoulder to contact the bottom surface of the work-piece[9]. The BTFSW is effective for joining hollow extrusions and lap joints[10]. The BTFSW appears promising for the joining of double curve fuselage components and the lightening of the welding clamping tool[11]. The BTFSW has been successfully used for many years in Japan for industrial fabrication of railway cars[6]. A bobbin tool consists of three parts: the upper shoulder, the pin (act similarly to the standard FSW) and the lower shoulder. Essentially, there are two types of bobbin or self-reacting techniques: technique of a fixed gap, between the shoulders and one that allows the gap between the shoulders to adapt during the welding operation, which is named as adaptive self-reacting friction stir welding (ASRFSW)[12]. However, BTFSW needs predrilled pilot holes during welding and has a risk of pin breakage when the welding energy is too low, and welds present lack of consolidation defects when the travel is too fast[8].

* Corresponding author. Assoc. Prof., Ph.D.; Tel.: +86 451 86413951; Fax: + 86 451 86416186; E-mail address: yxhuang@hit.edu.cn (Y. Huang).

http://dx.doi.org/10.1016/j.jmst.2014.04.009

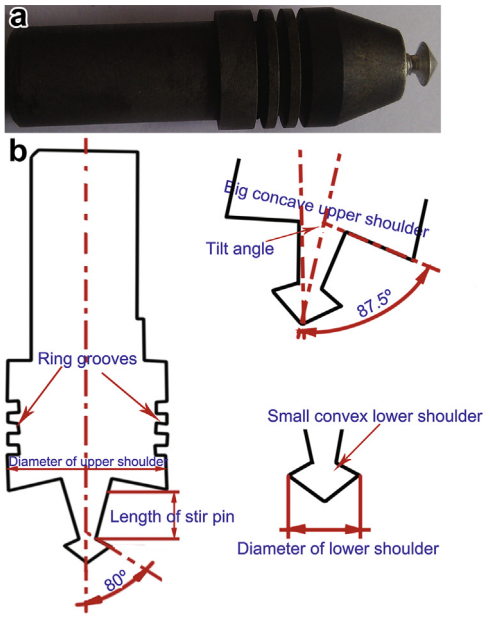

Fig. 1 Photos of SSFSW tool: (a) front view of SSFSW tool, (b) details of SSFSW tool.

For the FSW process, the characteristic of microstructural evolution and the resulting mechanical properties are determined by the thermal cycle and the material flow behavior. The formation quality of friction stir welded joints relies on the deformation ability and flow of the metal around the FSW tool[13]. The plastic deformation and temperature profile during FSW produce a microstructure characterized by a central weld nugget zone (WNZ) surrounded by a thermo-mechanically affected zone (TMAZ) and heat-affected zone (HAZ)[3]. The welded joint is fundamentally defect free and displays excellent mechanical properties when compared to conventional fusion welds[14,15]. Many researchers have done a lot of efforts to analyze the microstructural evolution[16−19]. However, only a few of investigations depict the microstructural characteristics and mechanical properties of BTFSW joints. Results show that BTFSW is better for medium and thick sections than for thin material[20,21], whereas other studies have achieved acceptable results for thin plate using bobbin tools[22,23]. It was reported by Lafly et al.[24] that the average tensile strength of the 6056-T78 aluminum alloy joint by adaptive self-reacting friction stir welding was 7%−20% lower than the conventional FSW joints. However, Marie et al.[7] pointed out that the tensile strength of the 6056-T78 aluminum alloy joints welded by SRFSW was equivalent to that of the conventional FSW joints. The optimized welding speeds at a constant rotation speed were concluded for ASRFSW dissimilar joints of 2219 and 2195 aluminum alloy by Skinner et al.[25], however, the microstructural development, tensile fracture location and the microhardness distribution of the joints were not reported. The high level substructure was observed in the TMAZ and low level substructure was observed in the WNZ in 6082-T6 aluminum alloy BTFSW joints by Threadgill et al.[26].

In the present work, a novel self-support FSW (SSFSW) tool, composed of the concave upper shoulder and the smaller convex lower shoulder, is developed to join the aluminum hollow extrusion. The effects of welding speed on the microstructure and mechanical properties of SSFSW joints welded at constant rotational speed are systematically investigated.

2. Experimental

All welding procedures were performed on 6082-T6 aluminum alloy plates with a thickness of 5 mm, width of 100 mm, and length of 300 mm. The chemical compositions of the alloy is (in wt%): 1.10 Mg, 0.80 Si, 0.60 Mn, 0.50 Fe, 0.25 Cr, 0.20 Zn, 0.10 Cu, 0.10 Ti with the balance made up of Al.

The SSFSW process were finished using FSW machine (FSW-3LM-003) with a rotational speed of 800 r/min, a tilt angle of 4°, and a plunge depth of 0.1 mm. The joining operation began with the preset welding parameters. Because of the introduction of lower shoulder, the extraction speed was 1 mm/min to prevent the pin breakage during the "tool extraction" process. The range of welding speed was 10−200 mm/min. The nonconsumable self-support tool composed of double shoulders (the concave upper shoulder and the smaller convex lower shoulder) made of high speed steel was used to fabricate the joints of aluminum hollow extrusion, as shown in Fig. 1. The diameter of the lower shoulder is smaller than that of the upper shoulder. The diameters of the upper shoulder and the lower shoulder are 14 and 9 mm, respectively. The length of the stir pin is 4.6 mm. The angle between the upper shoulder and tool center axis is 87.5°, and the angle between the lower shoulder and tool center axis is 80°.

The standard tensile samples of the joint were cut using super computer numerical control (CNC) wirecutting machine according to China national standard GB2651-2008 welding joint tensile test methods[27]. The room temperature tensile test was performed at a crosshead speed of 1 mm/min at an INSTRON-1186 universal testing machine. The fracture surfaces of tensile specimens were characterized by scanning electron microscopy (SEM, Hitachi-S4700) to understand the failure mode. The microhardness test was conducted by using a Vickers hardness testing machine (HX-1000) with a test load of 200 g and an indentation time of 10 s. As schematically shown in Fig. 2, a total of three test lines were measured across the cross-section, and the interval between two adjacent indentations on each line was 1 mm, with a total of 57 indentations.

Specimens were cut from the SSFSW welded plates to carry out microstructural and mechanical characterization. The specimens were prepared according to the standard procedures for specimen preparation including grinding, polishing and etching. The specimens were etched with reagent (1 ml hydrofluoric acid + 1.5 ml hydrochloric acid + 2.5 ml nitric acid + 95 ml water) to reveal the macro and microstructures. In order to analyze the microstructural evolution of the material, the cross-sections of welds were observed optically. The macro and microstructures of the joint were characterized by optical microscopy (OM, Olympus-MPG3) and scanning electron microscopy (SEM, Hitachi-S4700), respectively.

3. Results and Discussion

3.1. Macrostructure and microstructure of SSFSW joints

Low magnification optical macrographs of cross-section of SSFSW joints at the welding speed varied from 10 to 200 mm/min are shown in Fig. 3. All the joints exhibit three distinctive zones, i.e. heat-affected zone (HAZ), thermo-mechanically affected zone (TMAZ) and weld nugget zone (WNZ) as depicted in Fig. 3(a) and (d). In WNZ, the structure of band pattern is discernable. The upper part of the structure of band pattern is mainly influenced by the upper shoulder. The middle part of WNZ is mainly influenced

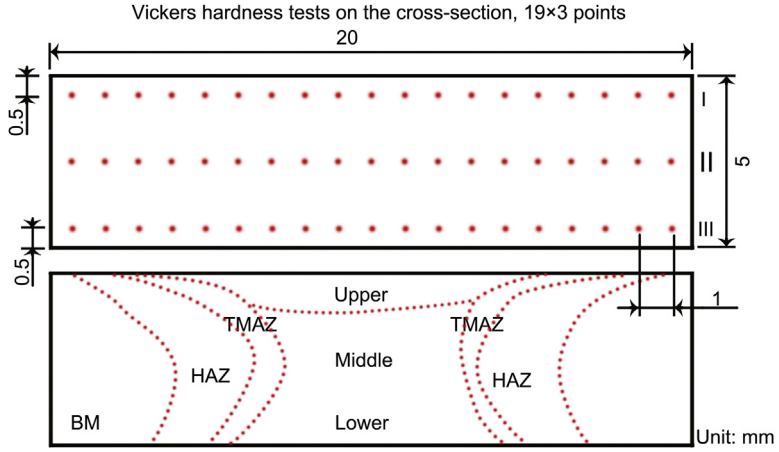

Fig. 2 Schematic illustration of the SSFSW joint for microhardness tests, together with an indication of various zones across the weld (BM, HAZ, TMAZ and WNZ).

by the stir pin and the lower part of WNZ is mainly influenced by the lower shoulder. The weld shape differs from the weld made from conventional FSW, and is slightly hourglass shaped. Such a shape is mainly determined by the material flowing during the SSFSW. The upper and lower surface experience extreme deformation and frictional heating by the contact with the upper and lower shoulder during SSFSW process, thereby resulting in such nugget zone. The interface between the recrystallized nugget zone and the parent metal is relatively diffuse on the retreating side (RS) of the SSFSW tool, but quite sharp on the advancing side (AS) of the tool, which is consistent with previous study[18]. The tunnel defect forms at the AS of the self-support friction stir welded joints. The size of the tunnel defect decreases with increasing welding speed. The formation of the weld defects at the top of the AS is closely related to the metal flow driven by shoulder extrusion and pin stirring. This observation also shows that the metal around the defects exhibits vortex-like flow features, which is often considered abnormal and should be avoided in FSW process, which causes disordered flow[13].

Single onion ring pattern observed in the welding nugget in the conventional FSW welds is replaced by series of onion rings stacked vertically through the thickness on the advancing side, as shown in Fig. 4(a−c). By employing a threaded tool, the plastic material is forced from the plate down into the weld and may travel several times depending on the rotational and welding speed[28]. Onion rings have alternate bright and dark rings. The gap between two consecutive rings at the center is wider than those at the outer edge. Onion rings found in the welded zone is a direct evidence of characteristic material transport phenomena occurring during SSFSW. The reduced stirring due to the higher speed or lower rotation speed will result in the partial breaking of natural Al_2O_3 oxide layer and low heat input retards flowability of plastic material. This weak flow causes localized presence of broken oxide particle in the form of dark wavy zigzag line or kissing bond defect, as shown in Fig. 4(d). It is imperative that a proper selection of welding parameters can effectively eliminate the formation of zigzag line, and even can change failure location from WNZ to TMAZ or HAZ, thus can improve mechanical performance of friction stir welded joints.

The WNZ comprises the material strongly affected by the tool rotation. It is subjected to a high level of plastic deformation and frictional heating. The upper part of WNZ is directly influenced by the stir pin and the concave upper shoulder, however, the lower part of WNZ is directly influenced by the stir pin and the convex lower shoulder. The highest strain and strain rates take place in WNZ[29,30]. Intense plastic deformation and frictional heating during FSW result in generation of a recrystallized fine-grained microstructure within stirred zone. Fig. 5 shows the typical cross-sectional second-phase particles distribution of the WNZ of the SSFSW joint. It can be seen that a considerable amount of constituent particles are randomly distributed in the base material (BM). However, there are far fewer second-phase particles in the nugget zone than in the BM. The second-phase particles in the WNZ are more uniform and intensive. There exist much more uniform and finer dispersoids (AlSiMnFe). The WNZ is surrounded by the TMAZ, having highly deformed and bent inhomogeneous coarser aluminum grains due to stirring by tool. The TMAZ grain structure appears to be bent towards the tool shoulders, as a result of material flow induced during the FSW. However, in this region plastic deformation and recrystallization are somewhat lesser than that in the weld nugget zone.

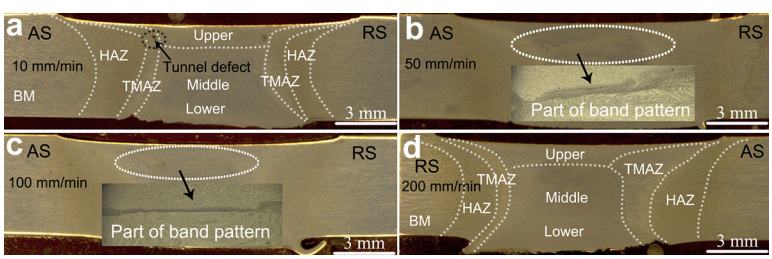

Fig. 3 Cross-sections of SSFSW joints welded for different welding speeds: (a) 10 mm/min, (b) 50 mm/min, (c) 100 mm/min, (d) 200 mm/min.

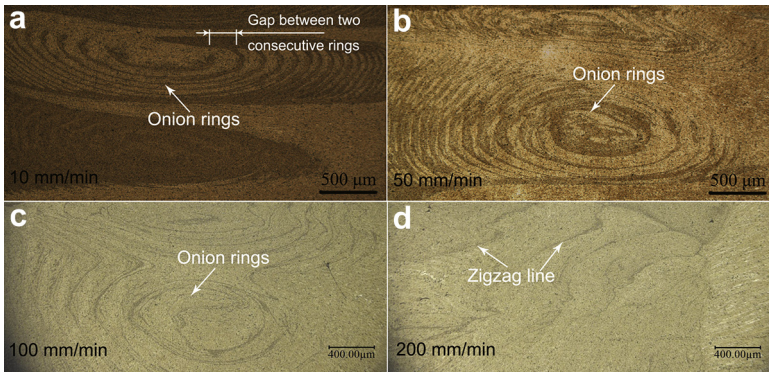

Fig. 4 Effect of welding speeds on the formation of onion ring and zigzag line: (a) 10 mm/min, (b) 50 mm/min, (c) 100 mm/min, (d) 200 mm/min.

The TMAZ consists of larger recrystallized grains than the WNZ on the AS, which is shown in Fig. 6. The regions bounded by dashed lines in Fig. 6 are a part of TMAZ. It has been suggested that the differences in microstructural observations may be resolved by considering a mechanism of continuous dynamic recrystallization in the TMAZ[31−33]. Fig. 7 shows the variation of the grain structure and grain size in HAZ according to the variation of distance from the center of the weld. In the HAZ, remote from the center of the weld, there is no obvious change in the grain structure compared with the base material, however, the grain size decreases with increasing distance to the weld centerline.

3.2. Mechanical properties of the SSFSW joints

The transverse microhardness distribution on the cross-sections of the joints is shown in Fig. 8. The microhardness of the BM is in the range of 100−105 HV. With respect to SSFSW joints, all the microhardness distribution profiles exhibit W-shape and are corresponding to three distinct microstructural zones. As seen, the microhardness falls dramatically in the region that is passed over by the shoulder and the microhardness reaches its lowest value in the softening region. The microhardness of TMAZ is lower than that of WNZ but higher than that of HAZ. Compared with HAZ, the increase of microhardness in TMAZ can be explained by the high density of dislocations which were induced by the plastic deformation during welding[34,35]. The minimum hardness is located at the interface between the TMAZ and HAZ. For all the joints welded at different welding speed from 10 to 200 mm/min, the microhardness in the WNZ is strongly reduced in contrast to the BM, indicating that thermal softening has occurred[9]. The microhardness of the WNZ has a growth tendency as the welding speed increases, because the grain size in the WNZ decreases with increasing welding speed and the age-hardening effect plays a certain role[35]. The values of microhardness have been improved at higher welding speed due to the decrease of the softened zone width.

The tensile properties of the joints as a function of welding speed are shown in Fig. 9. The tensile strength increases with increasing welding speed from 50 to 200 mm/min. The tensile strength reaches its maximum at the welding speed of 200 mm/min, and the corresponding joint efficiency is 69%. The joint ductility obeys the opponent tendency to the tensile strength, and its maximum value is 12.58%.

The fracture features of the joints welded at different welding speeds are shown in Fig. 10. The macro-fracture surface of tested specimen in tension presents 45° shear fracture along the tensile axis and the appearance indicates a ductile fracture mode. In the present study, the fracture occurs in the HAZ adjacent to the TMAZ on the AS, which is corresponding to the lowest hardness of the joint, as shown in Fig. 8. The fracture surfaces of tensile specimens are characterized using SEM to understand the failure mode, as shown in Fig. 11. From the results, it can be seen that they invariably consist of dimples, which indicates the specimens fail in ductile manner under the action of the tensile loading. Because fine dimples are the characteristic feature of ductile fracture, this feature validates the high ductility of the SSFSW joint during the tensile testing.

The above-mentioned results indicate that the welding speed has a significant effect on the mechanical properties of the SSFSW joints of 5-mm-thick 6082-T6 aluminum alloy. The welding speed influences the heat input per unit length of weld which controls the degree of softening and flowability of plasticized material[36]. On the one hand, at lower welding speed the amount of heat supplied to the deforming material in weld area is greater and therefore the softened area is wider around the

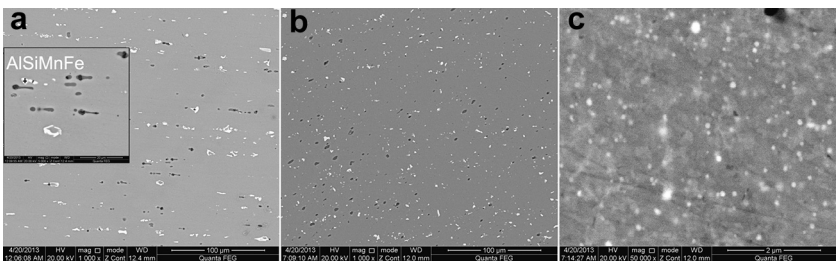

Fig. 5 Comparison of precipitates distribution: (a) base material, (b) WNZ, (c) higher magnification of WNZ.

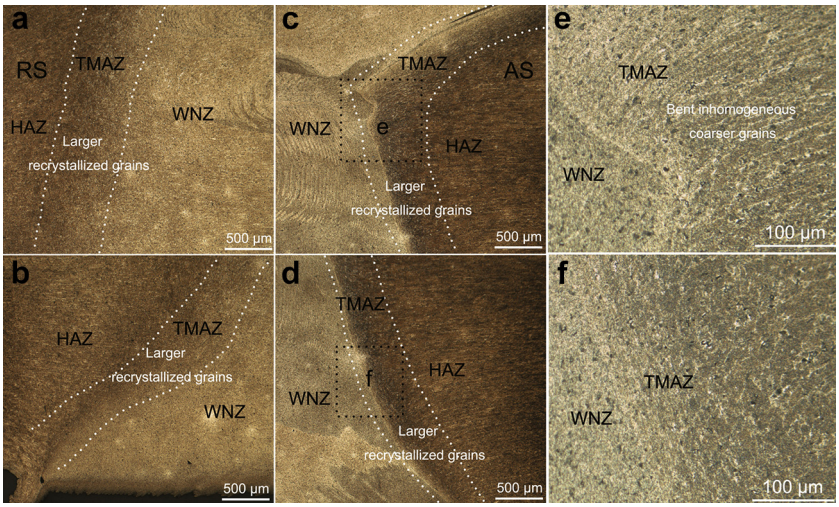

Fig. 6 Variation of microstructure of the SSFSW joint in different zones with the welding speed of 50 mm/min.

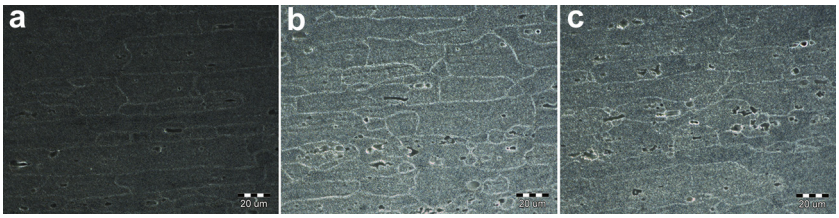

Fig. 7 Variation of grain size and morphology with increasing distance to the weld centerline in HAZ: (a) near the TMAZ, (b) middle region of the HAZ, (c) near the BM.

stirring tool leading to more improved metal flow and more effective bonding in the weld[36]. At high welding speed SSFSW tool results in lower heat input per unit length of weld which in turn reduces stirring of material. On the other hand, increasing welding speed can decrease the heat input into the joints, and thus reducing the coarsening and transformation of the precipitates[9]. In this case, the second-phase particles deterioration is weakened in the HAZ corresponding to failure location of the tensile specimen.

3.3. Flow pattern of softened material

As can be seen from Fig. 12, the structure of band pattern is discernable in the upper part of the WNZ from the AS to the WNZ center. This is consistent with the result reported by Horton[37]. They also observed the similar band pattern formed in the WNZ of the 2014/2219 dissimilar alloy BTFSW joints. Reynolds[38] thought that the unsteady flow of some sort must be the genesis of the cyclically varying microstructure observed in FSW. It is clear that there is a smooth narrow interface between WNZ and TMAZ on the AS compared with that on the RS, which is shown in Fig. 6. The plastic material in the TMAZ has flowed only a little into the region behind the pin on the AS, however, on the RS, such flow is greater because the rotating tool shears metal and additionally sweeps it resulting in a very irregular interface between TMAZ and nugget[39].

The upper and lower surface are in contact with the tool shoulders and therefore experience more frictional heating and plastic flow. It has been reported that the flow of the material near top surface layers of weld nuggets (up to a depth of about one third of weld thickness) is caused by FSW tool shoulder while that in sub-surface region occurs due to thread of the stir pin[40]. Therefore, flow pattern of the material near the top and

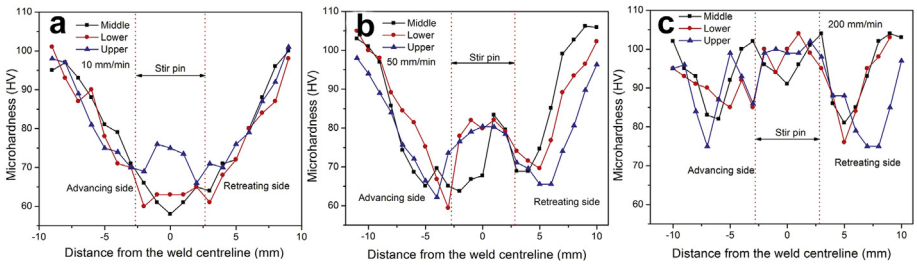

Fig. 8 Microhardness of the joints for different welding speeds: (a) 10 mm/min, (b) 50 mm/min, (c) 200 mm/min.

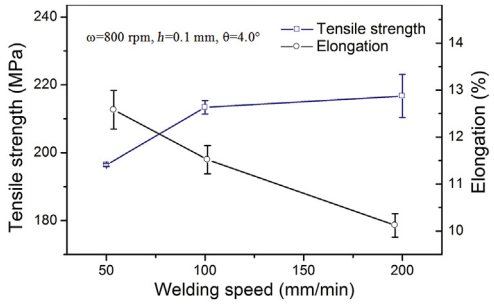

Fig. 9 Tensile properties of the joints for different welding speeds.

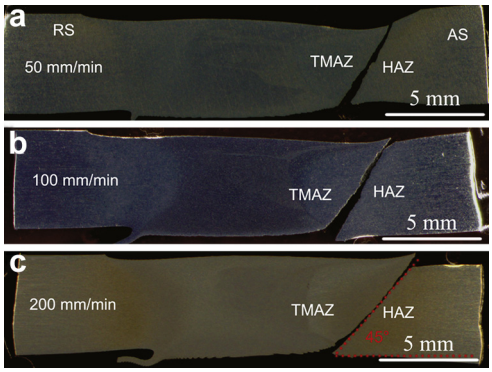

Fig. 10 Fracture features of the joints welded at different welding speeds: (a) 50 mm/min, (b) 100 mm/min, (c) 200 mm/min.

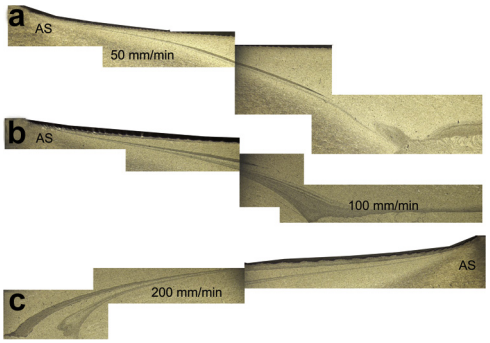

Fig. 12 Structure of band pattern at different welding speeds: (a) 50 mm/min, (b) 100 mm/min, (c) 200 mm/min.

the bottom of the weld surface becomes different from the middle part of the WNZ. As illustrated in Fig. 13, the weld zones of SSFSW joints are divided into three parts. The first is zone I, where the softened metal driven by the big concave upper shoulder occurs via a horizontal flow around the axle of the SSFSW tool. The second is zone II, where the softened metal driven by the screw thread on the pin is positioned upward in the spiral flow. The third is zone III, where the softened metal is driven by the small convex lower shoulder. The regions bounded by dashed lines in Fig. 13(b−d) are the locations of onion rings or zigzag line for those micrographs given in Fig. 4(b−d). The stacked onion ring features found in the WNZ are an evidence of the characteristic material transport occurring during SSFSW process. It means that the material transfer in the WNZ takes place layer by layer under the function of the SSFSW tool. In

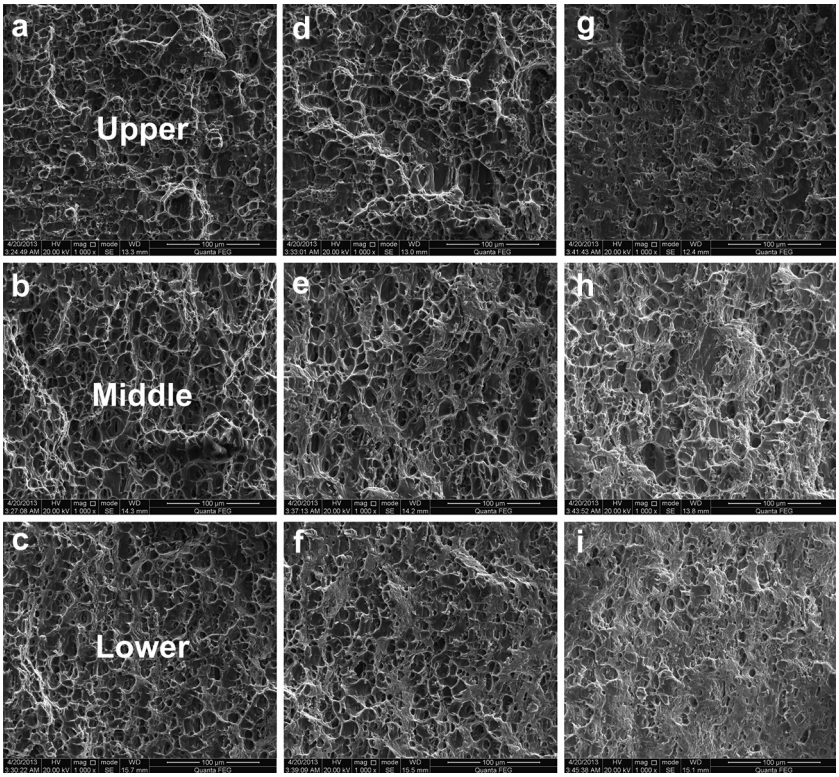

Fig. 11 Effect of welding speeds on fracture morphology: (a−c) 50 mm/min, (d−f) 100 mm/min, (g−i) 200 mm/min.

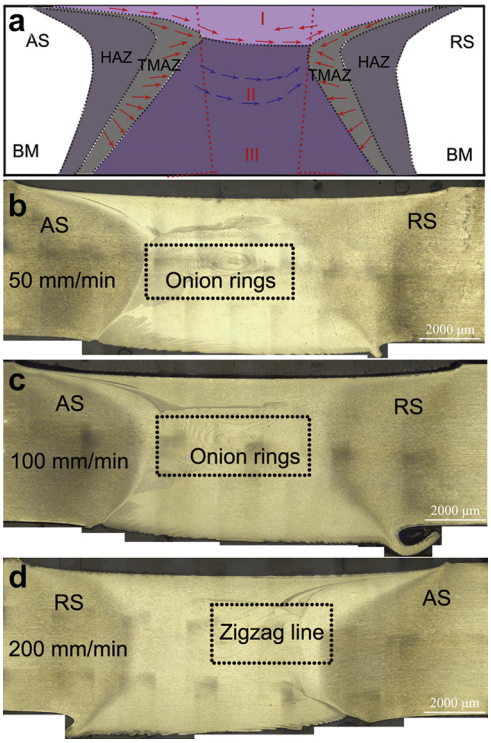

Fig. 13 Material flow around the SSFSW tool: (a) material plastic flow model for SSFSW, (b) 50 mm/min, (c) 100 mm/min, (d) 200 mm/min.

zone I, aside from the horizontal flow of the metal driven by the pressure force of the upper shoulder, an additional flow runs from upper surface to a depth of about one forth of weld thickness driven by the upper shoulder. In zone II, by employing a threaded tool the material is forced from the plate down into the weld and may travel several times depending on the rotational and welding speed. Material flow in the lower shoulder dominated zone is under study.

4. Conclusions

(1) The SSFSW tool, consisting of a big concave upper shoulder and a small convex lower shoulder, is developed to join aluminum hollow extrusion. The typical weld shape of the SSFSW joint differs from the conventional FSW joint, and is slightly hourglass shaped.

(2) Single onion ring pattern observed in the welding nugget in the conventional FSW welds is replaced by series of onion rings stacked vertically through the thickness on the advancing side, and the weak flow causes localized presence of broken oxide particle in the form of dark wavy zigzag line or kissing bond defect during SSFSW process.

(3) The welding speed plays an important role in weld quality during SSFSW. The effect of welding speed on mechanical properties of the joints was investigated. The tensile strength of the SSFSW joint increases with the welding speed, and the maximum tensile strength is equivalent to 69% of that of the BM. The values of microhardness of SSFSW joints increased with increasing welding speed from 10 to 200 mm/min. The tensile fracture location is in the HAZ adjacent to the TMAZ on the AS and the tensile specimens present ductile failure.

(4) The structure of band pattern exists in the upper part of the WNZ from the AS to the WNZ center due to the unsteady flow of plastic material and there is a smooth narrow interface between WNZ and TMAZ on the AS compared with that on the RS. The weld zones of SSFSW joints are divided into three parts due to the introduction of the lower shoulder. It is essential to fabricate defect-free SSFSW joints via controlling flow patterns of the metal around the stir tool.

Acknowledgments

The work was jointly supported by the National Natural Science Foundation of China (Nos. 50904020 and 50974046) and the Fundamental Research Funds for the Central Universities (No. HIT. NSRIF. 2012007).

REFERENCES

[1] W.M. Thomas, E.D. Nicholas, J.C. Needham, M.G. Murch, P. Templesmith C.J. Dawes, Patent Appl. No. PCT/GB92102203 and Great Britain Patent Appl. No. 9125978.8, 1991.
[2] S. Babu, G.D. Janaki Ram, P.V. Venkitakrishnan, G. Madhusudhan Reddy, K. Prasad Rao, J. Mater. Sci. Technol. 28 (2012) 414−426.
[3] C. Hamilton, S. Dymek, A. Sommers, Weld. J. 89 (2010) 189−194.
[4] T. Kawasaki, T. Makino, K. Masai, H. Ohba, Y. Ina, M. Ezumi, JSME Int. J. 47 (2004) 502−511.
[5] H. Ohba, C. Ueda, K. Agatsuma, Hitachi. Rev. 50 (2001) 130−133.
[6] Y.X. Huang, L. Wan, S.X. Lv, J.C. Feng, Sci. Technol. Weld. Join. 18 (2013) 239−246.
[7] F. Marie, D. Allehaux, B. Esmiller, in: Fifth International Symposium on Friction Stir Welding, Metz, France, September 14−16, 2004.
[8] F. Marie, B. Guerin, D. Deloison, D. Aliaga, in: Seventh International Symposium on Friction Stir Welding, Awaji Island, Japan, May 20−22, 2008.
[9] H.J. Liu, J.C. Hou, H. Guo, Mater. Des. 50 (2013) 872−878.
[10] W.M. Thomas, C.S. Wiesner, D.J. Marks, D.G. Staines, Sci. Technol. Weld. Join. 14 (2009) 247−253.
[11] D. Alléhaux, F. Marie, Mater. Sci. Forum 519−521 (2006) 1131−1138.
[12] J. Hilgert, H.N.B. Schmidt, J.F. dos Santos, N. Huber, J. Mater. Process. Technol. 211 (2011) 197−204.
[13] R.D. Fu, R.C. Sun, F.C. Zhang, H.J. Liu, Weld. J. 91 (2012) 169−173.
[14] M.A. Sutton, B.C. Yang, A.P. Reynolds, J.H. Yan, Mater. Sci. Eng. A 364 (2004) 66−74.
[15] D.Q. Wang, S.H. Liu, Z.X. Cao, J. Mater. Sci. 39 (2004) 1689−1693.
[16] W. Woo, L. Balogh, T. Ungár, H. Choo, Z.L. Feng, Mater. Sci. Eng. A 498 (2008) 308−313.
[17] U.F.H.R. Suhuddin, S. Mironov, Y.S. Sato, H. Kokawa, Mater. Sci. Eng. A 527 (2010) 1962−1969.
[18] R.S. Mishra, Z.Y. Ma, Mater. Sci. Eng. R 50 (2005) 1−78.
[19] H.B. Chen, K. Yan, T. Lin, S.B. Chen, C.Y. Jiang, Y. Zhao, Mater. Sci. Eng. A 433 (2006) 64−69.
[20] K.J. Colligan, A.K. O'Donnell, J.W. Shevock, M.T. Smitherman, in: 9th International Symposium of Friction Stir Welding, Von Braun Center, Huntsville, Alabama, U.S., TWI Limited, 2012.
[21] G. Sylva, R. Edwards, T. Sassa, in: Proceedings of 5th International Friction Stir Welding Symposiunm, Metz, France, September, 2004.
[22] R. Edwards, G. Sylva, in: 7th International Conference on Trends in Welding Research, Pine Mountain, GA, U.S., May 16−20, 2005.

[23] T. Neumann, R. Zettler, P. Vilaca, J.F. dos Santos, L. Quintino, Friction Stir Weld Process IV, 2007, pp. 171−176.
[24] A.L. Lafly, D. Alléhaux, F. Marine, C.D. Donne, H. Döker, Weld. World 50 (2006) 1−13.
[25] M. Skinner, R.L. Edwards, G. Adams, Z.X. Li, Mater. Sci. Forum 426−432 (2003) 2849−2854.
[26] P.L. Threadgill, M.M.Z. Ahmed, J.P. Martin, J.G. Perrett, B. P. Wynne, Mater. Sci. Forum 638−624 (2010) 1179−1184.
[27] GB/T 2651, Tensile Test Method on Welded Joints, Standardization Administration of the People's Republic of China, 2008 (in Chinese).
[28] P. Cavaliere, A. De Santis, F. Panella, A. Squillace, Mater. Des. 30 (2009) 609−616.
[29] W.F. Xu, J.H. Liu, H.Q. Zhu, F. Li, Mater. Des. 47 (2013) 599−606.
[30] W.F. Xu, J.H. Liu, G.H. Luan, C.L. Dong, Mater. Des. 30 (2009) 1886−1893.
[31] J.Q. Su, T.W. Nelson, R. Mishra, M. Mahoney, Acta Mater. 51 (2003) 713−729.
[32] K.V. Jata, K.K. Sankaran, J.J. Ruschau, Metall. Trans. A 31 (2000) 2181−2192.
[33] K.V. Jata, S.L. Semiatin, Scripta Mater. 43 (2000) 743−749.
[34] W.S. Miller, L. Zhuang, J. Bottema, A.J. Wittebrood, P. Smet, A. De Haszler, Mater. Sci. Eng. A 280 (2000) 37−49.
[35] P. Dong, H.M. Li, D.Q. Sun, W.B. Gong, J. Liu, Mater. Des. 45 (2013) 524−531.
[36] C. Sharma, K.D. Dheerendra, K. Pradeep, Mater. Des. 36 (2012) 379−390.
[37] K.R. Horton, Micro-hardness, Strength and Strain Field Characterization of Self-reacting Friction Stir and Plug Welds of Dissimilar Aluminum Alloys, Ph.D. Thesis, the University of Alabama, Tuscaloosa, 2011.
[38] A.P. Reynolds, Scripta Mater. 58 (2008) 338−342.
[39] M. Cabibbo, H.J. McQueen, E. Evangelista, S. Spigarelli, M. Di Paola, A. Falchero, Mater. Sci. Eng. A 460−461 (2007) 86−94.
[40] M. Guerra, C. Schmidt, J.C. McClure, L.E. Murr, A.C. Nunes, Mater. Charact. 49 (2003) 95−101.